Approach to Large Space Structure Control System Design Using Traditional Tools

P. Y. Chu,* B. Wie,† B. Gretz,‡ and C. Plescia§
Ford Aerospace Corporation, Palo Alto, California

This paper illustrates how traditional analysis and design tools can be successfully applied, with insights derived from recent research on control-structure interaction, to preliminary control system design for a large space structure such as the Space Station Freedom. The control system regulates attitude during construction, normal on-orbit operation, reboost, and docking using control-moment gyros and thrusters. The tools include finite-element modeling, model reduction based on modal truncation, single-input/single-output Bode plot design, position and rate feedback, roll-off and phase filter, and simulation. The resulting system is characterized by simple architecture and moderate bandwidth. The large configuration changes during the construction period are handled by gain scheduling.

Introduction

PHASE 1 of the space station (Fig. 1) is scheduled to be built in the late 1990s. It features a truss structure 460 ft long to which are attached several large flexible solar arrays and radiators as well as habitable modules. The operational orbit is 180 to 250 n.mi. Most likely, it will be the largest spacecraft in orbit for the next several decades.

The space station requires a control system to maintain attitude stability in all phases of construction and operation. The control system must handle disturbances from crew activity, machinery motion, vehicle docking, and orbit reboost. Furthermore, the space station configurations change as payloads and modules are moved, as Shuttles and other spacecraft are docked, as supplies and fuel are transferred, and as satellites are assembled or serviced. The control system must either be robust or adjust to the changes.

When a designer is faced with such a large structure and the set of mission requirements, one question arises naturally: Are my tools adequate for the design task? This paper describes the process of a design exercise[1] that shows traditional tools, consisting of NASTRAN modeling, modal residue model reduction, sensor/actuator modeling, single-input/single-output classical control design, gain scheduling based on inertia changes, and simulation, can be satisfactory at least for the preliminary design phase if the designer uses insights derived from recent research on control-structure interaction.

Modeling and Design Methodologies

Structural Modeling

The modeling process for a large space structure like the space station can be grouped into six steps: analyze rigid-body characteristics, perform finite-element analysis, obtain linear dynamic equations, transform among various forms, generate plots, and reduce model order. The equation of motion for an undamped structure is given by

$$M\ddot{x} + Kx = f \tag{1}$$

where x is the translational and angular displacement vector of the nodes, f the external force or torque vector, M the mass matrix, and K the stiffness matrix. Equation (1) can be transformed into the normalized modal equation

$$\ddot{\eta} + \Omega^2\eta = P^T f, \qquad x = P\eta \tag{2}$$

where η is the modal coordinate vector, P the eigenvector matrix, and $\Omega^2 = \text{diag}(\omega^2)$ the diagonal modal frequency matrix. The formulation of Eqs. (1) and (2) is often done with a finite-element analysis program such as NASTRAN.[2] The modal frequencies and modal displacements at nodes such as sensors, actuators, payloads, and disturbance sources are then extracted to a control design software package. The modal state-space form in Eq. (2) is equivalent to the transfer-function pole/residue form

$$y = H\left[\sum_{i=1}^{n} \frac{P_i P_i^T}{s^2 + \omega_i^2}\right] Q \tag{3}$$

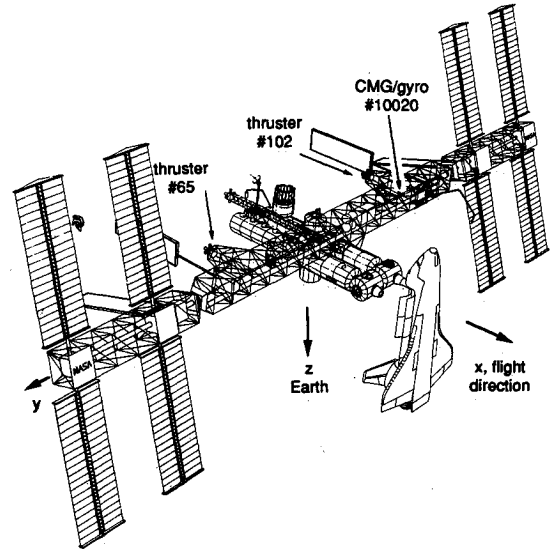

Fig. 1 Coordinate system and sensor and actuator locations of the phase 1 space station.

Received March 31, 1989; revision received March 22, 1990.

*Senior Engineering Specialist. Member AIAA.
†Consultant; currently Associate Professor, Department of Mechanical and Aerospace Engineering, Arizona State University, Tempe, AZ. Member AIAA.
‡R&D Engineer; currently with University of Pennsylvania, Philadelphia, PA. Member AIAA.
§Principal Engineer.

where n is the number of modes, P_i the ith eigenvector, H the output distribution matrix, and y the output vector. Equations (2) and (3) are the best forms for describing lightly damped high-order systems. Other equivalent forms such as first-order state space are not as convenient or numerically reliable.[3]

Cross checks should be applied to establish confidence in the modeling process. The first few modes often can be traced to solar arrays or long trusses. Modal displacements of the six rigid-body modes should be consistent with the static mass properties.[1] Confusions often arise because structural and control engineers use different coordinate systems, units, and definitions of terms such as the products of inertia.

The open- and closed-loop transfer functions are usually analyzed using graphical tools such as residue bar charts, Bode plots, pole/zero plots, root-locus plots, and Nyquist plots. Much of the currently available software for these plots has difficulty being both reliable and efficient when dealing with high-order systems. We had to develop a custom procedure to consistently show on Bode plots the rigid-body mode, the width of the valley due to the first zero, the heights of major peaks, and phase excursions beyond the ± 180 deg range.[1]

Model Order Reduction

The first step in the model-reduction process actually occurs during finite-element modeling. The model should not be so detailed that the calculated frequencies are crowded with local modes. Even so, finite-element runs often produce hundreds of modes within the frequencies of interest. For example, a NASTRAN run[4] used as the primary model in this study produced 124 structural modes below 10 Hz. Simulation checks have shown that only 17 modes in addition to the rigid-body modes are needed to adequately represent the three-axis time-domain behavior. The control design described later only needs six to eight modes in each axis.

Pole/zero cancellations and modal truncations are the traditional model-reduction methods for SISO (single-input/single-output) systems. Almost all methods for order reduction use some form of a threshold criterion,[5] whose numerical value is determined by engineering judgment. These methods do not closely interact with the controller synthesis process and thus tend to retain too many modes. The balanced realization method based on the concept of controllability and observability has been popular. This method generally changes all poles, zeros, and residues. A direct numerical optimization approach based on the pole/residue form has recently been developed.[6] For lightly damped space structures with sufficient modal separation, Bernard[3] shows that various model-reduction approaches in the literature are equivalent to modal truncation using different modal indices. The best index seems to be $\bar{\sigma}(R_i)/\zeta\omega_i$, where $\bar{\sigma}$ is the largest singular value, ζ the damping ratio, ω_i the ith modal frequency, and $R_i = P_i P_i^T$ the ith residue matrix.[3]

The model-reduction method to be described here is directly related to the SISO Bode-plot-based design approach. Reduction is performed on individual SISO transfer functions. Emphasis is placed on retaining high peaks because they usually determine the gain margins. Retaining the general shape of the Bode plot in the low-frequency range is also emphasized to allow accurate analysis of phase margin and bandwidth. Because only a small number of modes are retained, this method selects the modes to keep rather than to remove. A list of mode sequence number, frequency ω, residue r, $r/\zeta\omega$ [for $\bar{\sigma}(R) = r$], and $r/2\zeta\omega^2$ (for peak magnitude) accompanying the plots can reduce the chance for mistakes and speed up the later design process.

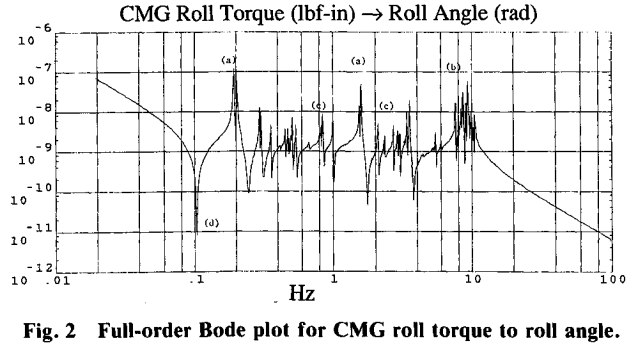

Fig. 2 Full-order Bode plot for CMG roll torque to roll angle.

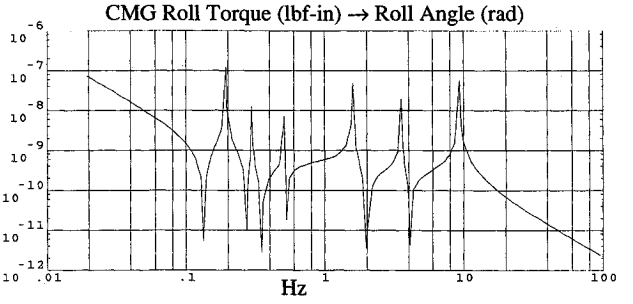

Fig. 3 Reduced-order Bode plot for CMG roll torque to roll angle.

Table 1 Characteristics of gain and phase stabilization

Characteristics	Stabilization approach	
	Gain stabilization	Phase stabilization
Feedback processing	Magnitude attenuation	Phase shift
Effect on damping	No change	Increase
Critical margin	Gain	Phase
Filters	Notch, roll-off	1st/2nd order lead/lag

Before model reduction is started, form an idea of how a rigid-body compensator would alter the full-order open-loop Bode plot, the desired bandwidth, and whether gain- or phase-stabilization is to be used for the flexible modes. This step helps retain more critical features in the crossover region and remove more modes in higher frequencies. This is a practice of the common notion that model reduction and control synthesis are related, and is also a practice of the frequency-weighted model-reduction methodology.

Figure 2 is the full-order Bode plot of the transfer function from the control moment gyro (CMG) roll torque to the collocated sensor output roll angle. On the magnitude plot, the peaks that clearly stand out (feature a) are retained. If a group of high peaks clusters together, only the highest one is retained (feature b). Those deleted may actually have a significant contribution to input-output relations, but the influence of the group as a whole can be represented by the highest peak for the purpose of assessing stability. Other model-reduction methods tend to keep all modes in such a cluster.

A distinct medium-height peak can be deleted if it is between other higher peaks and the anticipated compensated curve does not have a sharp turn there (feature c). In the mid-frequency region, where the gain curve (including compensator) is expected to cross the 0 dB line or the phase curve to cross the -180 deg line, keep a mode if in doubt. Be especially conservative if the phase curve in the region has consecutive phase jumps in the same direction. This occurs only when the sensor and actuator are not collocated.

The reduced-order Bode plot is then plotted (Fig. 3) and compared with the full-order plot in both magnitude and phase. If the first few important zeros (feature d) have moved significantly and they are expected to interact with phase compensators or influence phase margins, transform the reduced model to pole/zero form and substitute these new zeros by their corresponding original zeros shown on the full-order plot. The patched model is then transformed back to the pole/residue form and the overall gain is adjusted to match the rigid-body mode with the original one. The resulting changes of peak magnitudes must be noted and factored into the gain margin calculation.

Table 2 Major features and evolving trend of the five representative space station buildup stages (Ref. 4)[a]

Data set name	06B	07C	08A	09A	10
Flight no.	1	2	5	8	13
Description			Man-tended	Permanently manned	Phase 1
Module additions	Half-truss 1 solar array	Half-truss 1 solar array	Laboratory 2 radiators RMS, stinger	Habitation logistics	European Japanese 2 solar arrays
Mass, 1000 lb	42	82	173	287	427
Inertia, 10^{10} lbm-in.^{2}					
x	2.8	12	14	15	36
y	0.27	0.53	1.8	3.4	7.6
z	2.7	11	14	16	38
Total length, ft					
x	67	67	130	138	138
y	180	344	344	344	459
z	186	186	186	186	186
First mode, Hz	0.48	0.36	0.33	0.325	0.19

[a]The latest baseline assembly sequence has been changed.

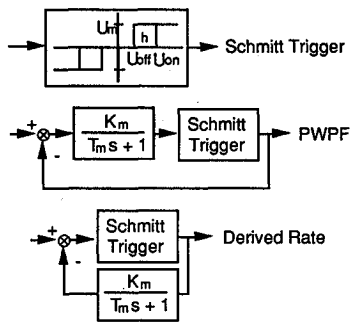

Fig. 4 Thruster modulator candidates.

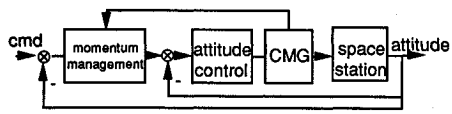

Fig. 5 Block diagram of attitude controller and momentum management system.

Control Loop Design

The two major ways to stabilize a system are gain- and phase-stabilization, the characteristics of which are summarized in Table 1. The controller synthesis approach in this study is based on the classical Bode plot. However, it is also enhanced by the results of the "modern" control theory.[7] The first step is applying a position-rate feedback (or a lead filter) to stabilize the rigid-body mode and achieve the desired bandwidth. Considerations in selecting the bandwidth include performance requirements, noise sensitivities, and control authorities. The issues invariably involve other subsystems and are subject to system engineering tradeoffs.

The second step is to add a first- or second-order low-pass filter depending on the amount of attenuation required for the high-frequency peaks. The corner frequency is selected as low as possible without causing significant distortion of the phase curve near the -180 deg crossover. It leaves only a few structural modes lacking sufficient stability margins in low (and occasionally medium) frequencies. For each such mode or mode cluster, starting at the low-frequency end, a second-order filter is selected from a menu[8] that shapes the gain and phase curves to provide adequate margins. The menu consists of lead, lag, phase notch, gain notch, and nonminimum phase filters. The last category provides a 360 deg phase excursion for difficult open-loop phase characteristics arising from noncollocated sensor/actuator pairs. Filters with a wide phase "hump" instead of a sharp magnitude notch are preferred because they are more robust to modal frequency variations.

This methodology can be extended to synthesis of a linear controller for a reaction jet system when the on-off nature of thrusters is linearized by modulators such as PWPF (pulse-width-pulse-frequency) or derived rate (Fig. 4). However, when a Schmitt trigger replaces the modulator, many aspects of the behavior of the closed-loop system are retained. In any event, the design should be augmented with nonlinear stability analysis and extensive simulation.

Preliminary Space Station Attitude Control System Design

Table 2 shows the features, evolving trend, and basic mass properties of the five major space station buildup configurations. Angles and angular rates are estimated by an attitude determination system that is based on low-noise gyros with updates from star sensors. Control moment gyros are the main torquing devices and share the same general locations with the attitude determination system (Fig. 1). Neither the CMG dynamics nor their steering law[9] is modeled in this study because the CMGs have a bandwidth in excess of 3 Hz. Therefore, whether the CMGs are double- or single-gimbaled does not affect the results of this study. The peak torque for each gimbal is at least 200 ft-lb. The 25-lb reaction control system (RCS) thrusters are aligned with the x-y-z axes.

The space station is designed to be a platform on which specific payloads maintain fine-pointing through their own control systems. A preliminary document[10] specifies an attitude limit of ± 1 deg/axis relative to the torque equilibrium attitude (which can be ± 5 deg from local-vertical-local-horizontal) and an attitude rate limit of ± 0.0005 deg/s per axis during normal mode operation. These specifications were not taken as requirements. The goal of this study is to find the upper bound of the bandwidth for the given structure while providing sufficient robustness for the configuration changes described earlier. The resulting design minimizes the attitude transients for a set of representative disturbance scenarios.

The attitude control system for the space station can be separated into two parts:

1) For routine on-orbit flight, the normal mode controller uses the CMGs as actuators and the gyros as sensors to maintain attitude stability. Common mode serves the period before completion of construction but after the CMGs have been

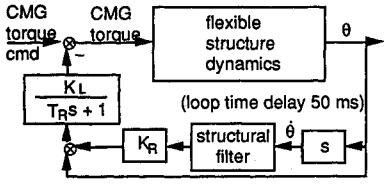

Fig. 6 Roll and yaw normal mode block diagram.

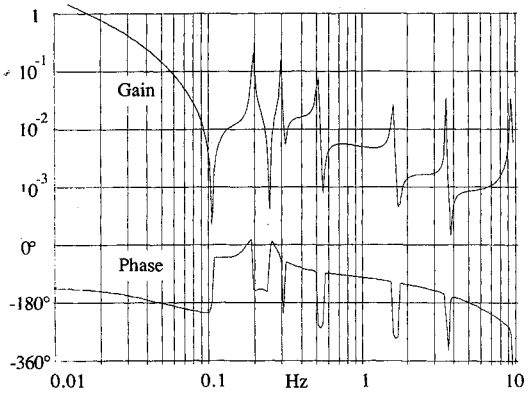

Fig. 7 Normal mode roll Bode plot with compensator and reduced-order model.

installed (see Table 2). It uses a similar control topology with scheduled gain sets and a reduced bandwidth. The momentum management system that prevents momentum buildup in the CMGs is regarded as an outer loop (see Fig. 5) and is the subject of other studies.[10-12] Since the CMG mode reported here has a time constant of about 2 min while that of the momentum management system is about 1 h, the two systems can be designed separately.

2) During orbit reboost, the RCS controller uses the thrusters near the main truss as the actuators and the gyros as sensors. This controller is also used in docking mode to attenuate impulsive docking disturbances. A similar controller is used as the attitude hold mode. It always operates in the background with a large deadband to back up the CMG mode against failures or disturbances that cause CMG saturation. A tight-pointing attitude hold mode has also been developed for specialized tasks.

Control Moment Gyro Normal Mode

Control moment gyro mode design is impacted primarily by the low-frequency modes associated with the main truss and solar arrays. Because the open-loop frequency responses of the roll and yaw axes are similar, the same controller topology is used for both. Figure 6 shows a block diagram of this controller. Figure 7 shows the roll-axis Bode plot using the reduced-order model. The loop gain gives a bandwidth exceeding 0.01 Hz. At this frequency, the rate gain provides a rigid-body phase margin of about 40 deg. The second-order roll-off filter with a corner frequency of 0.33 Hz begins to decrease the phase above the bandwidth. However, its gain attenuation ensures that structural modes above about 1 Hz are gain-stabilized.

Because of phase degradation from the roll-off filter on the fundamental structural mode, the gain margin of the first mode is insufficient. Lowering the roll-off filter corner to attenuate the mode further will reduce the rigid-body bandwidth and phase margin. A simple controller that satisfies the space station pointing requirements would have resulted at this stage; however, high bandwidth was set as a design goal. A more complicated roll-off filter would help attenuate magnitude more sharply, but the phase degradation on the first few modes would make the approach difficult and often fruitless. Instead, the second-order filter

$$\frac{(s/\omega_z)^2 + (2\zeta_z s/\omega_z) + 1}{(s/\omega_p)^2 + (2\zeta_p s/\omega_p) + 1} \tag{4}$$

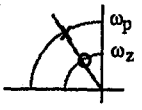

is adopted here to phase-stabilize the mode and maintain adequate phase margin. This "phase lead" filter has a relatively wide phase "hump" near its effective region that covers the possible variations of the phase drop between the first pole and the second zero.[13] Such a filter may also stabilize several adjacent modes.

No other structural modes are actively stabilized. Between the second mode and 1 Hz, there is a trade-off between the closed-loop bandwidth and compensator complexity. Furthermore, active phase-stabilization in this region necessarily results in highly tuned filters sensitive to plant variations. For the modes higher than 1 Hz, the phase loss due to loop time delay is too much. Adjustments to the roll-off filter to gain-stabilize these high-frequency modes avoid these difficulties. After several iterations, the controller gives a bandwidth as high as 0.016 Hz for both the roll and yaw axes.

Unlike the roll and yaw axes, the torsional flexibility of the truss and extensions of the solar arrays and radiators results in many closely spaced structural resonances extended to high frequencies on the pitch axis. Therefore, the pitch controller is designed to provide a somewhat lower closed-loop bandwidth than that of roll and yaw. Figure 8 shows a block diagram of the pitch controller and Fig. 9 shows the pitch Bode plot with the compensator and reduced-order model. The low loop gain and the first-order roll-off filter gain-stabilize all structural modes and give a pitch loop bandwidth of 0.01 Hz. The rate gain provides a rigid-body phase margin of about 35 deg. A higher bandwidth can be achieved only with great difficulty due to the large structural resonances at very high frequencies. Phase stabilization is undesirable because the structural modes are spaced too closely and would require highly tuned filters. Table 3 gives the normal mode controller gains and parameters, Table 4 the closed-loop pole locations, and Table 5 the stability margins. The high peak at 3.9 Hz caused a small 5.5 dB gain margin, which is not a real concern because the CMG bandwidth of about 3 Hz can provide additional roll-off.

Time responses are generated using a coupled three-axis simulation that includes 17 structural modes. A large crew

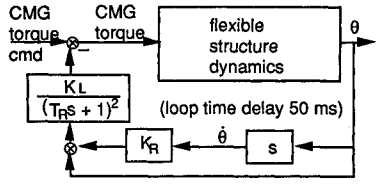

Fig. 8 Pitch normal mode controller block diagram.

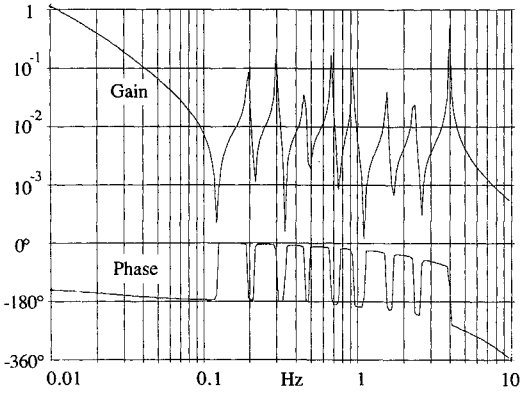

Fig. 9 Normal mode pitch Bode plot with compensator and reduced-order model.

Table 3 Normal mode controller parameters

Parameter	Description	Roll	Pitch	Yaw
K_r	rate gain, s	35	40	35
K_l	loop gain, lb-in./rad	3.0×10^6	0.4×10^6	3.5×10^6
T_r	roll-off, s	3	10	3
ω_z	filter zero, Hz	0.18	—	0.18
ω_p	filter pole, Hz	0.27	—	0.30
ζ	filter damping	0.15	—	0.20

Table 4 Normal mode closed-loop rigid-body poles

	Roll	Pitch	Yaw
ω, rad/s	0.13	0.08	0.14
ζ	0.50	0.42	0.47

Table 5 Normal mode stability margins

	Roll	Pitch	Yaw
Rigid-body phase margin, deg	40	35	40
Rigid-body gain margin, dB	17	∞	15
Flex phase margin, deg[a]	100 @ 0.19 Hz	∞	65 @ 0.20 Hz
Flex gain margin, dB[b]	7.4 @ 0.51 Hz	5.5 @ 3.9 Hz	13 @ 3.9 Hz

[a]Assuming 50 ms loop time delay.
[b]Assuming 0.002 natural damping ratio.

Table 6 Schedule for common mode loop gain K_L (10^5 lb-in./rad)

Flight	Roll	Pitch	Yaw
2	17	0.35	7
5	17	1.2	7
8	18	1.6	8

Rate gain $K_R = 20$ s.
Roll-off corner $T_R = 0.6$ s.

disturbance is modeled as a 33.7 lbf-s impulse.[14] Such a disturbance could occur during extravehicular activities when an astronaut pushes forcefully off an external wall. The simulation (Fig. 10) shows structural modes being excited and attenuated, with the rigid-body mode dominating the transients. The maximum control torque command is about 200 ft-lb, near the torque capacity of a single CMG. Because the roll and yaw bandwidths have been intentionally kept high, they could be lowered in the actual space station to be similar to the pitch bandwidth. Transient time would be 100 s and the maximum CMG torque 100 ft-lb. Using torque limiters on the high bandwidth design would have a similar effect. Other crew activities such as console operation create low-amplitude disturbances with frequencies in excess of 0.2 Hz,[14] which are more than an order of magnitude above the control bandwidth. Virtually no control response is caused by these activities. Inertia changes due to the mobile transporter are not assessed in this study, but were treated in Ref. 12.

Control Moment Gyro Common Mode

Common mode is used for attitude control for the period between the installation of CMGs and gyros at the second flight and when the phase 1 final configuration is reached. The common mode controller must remain functional in the presence of large inertia and structural frequency variations that occur as the space station is assembled. The roll and yaw inertias increase by a factor of 3 and the pitch inertia by 7, whereas the fundamental frequency decreases by a factor of 2 (see Table 2). The control system must be robust enough to handle "small" plant variations such as those that occur between Shuttle flights and adjustable to handle "large" plant variations that occur during module installation. The solutions adopted here are lowering the bandwidth, attenuating all flexible modes to ensure robustness, and selecting loop gain changes as functions of inertia.

The common mode topology on all three axes is identical to that of the normal mode pitch controller. A bandwidth of 0.008 Hz, which gives a settling time of 120 s, is used on all three axes in all configurations. The rigid-body phase margin is 45 deg and the damping ratio of the closed-loop rigid-body mode is 0.5. All flexible mode gain margins exceed 17 dB. Flights 2 to 5 share the same gain set on the roll and yaw axes. Flight 8 may use an optional small-position gain increase to maintain the bandwidth, whereas flight 9 needs no further adjustment. From flight 2 to flight 8, the pitch position gain is indexed to pitch inertia, while all other gains stay the same. The closed-loop performance for the common mode is roughly the same on all three axes. Table 6 lists the common mode gain schedule.

RCS Modes

The thrusters are not collocated with the sensor package and thus, as shown in Fig. 11, the poles and zeros no longer alternate. In addition, reaction jets cannot be throttled linearly. However, thruster modulators such as pulse-width-pulse-frequency (PWPF)[13] or derived rate can linearize the thruster behavior. Analyses have shown that many important closed-loop characteristics do not change even when the modulator is replaced by a Schmitt trigger. This conclusion allows the CMG mode design process to be extended for RCS mode design.[1]

The basic design driver for the RCS mode is the thruster distribution. As shown in Fig. 1, a thrust at NASTRAN node no. 65 along the z axis produces a positive roll and pitch torque. This strong coupling can be resolved by the reboost mode controller as shown in Fig. 12, where a positive roll error causes no. 65 to produce a negative z thrust and no. 102 to produce a positive z thrust, thereby canceling the pitch torques. A more mathematical approach using the inertia matrix and thruster torque matrix would have led to a similar

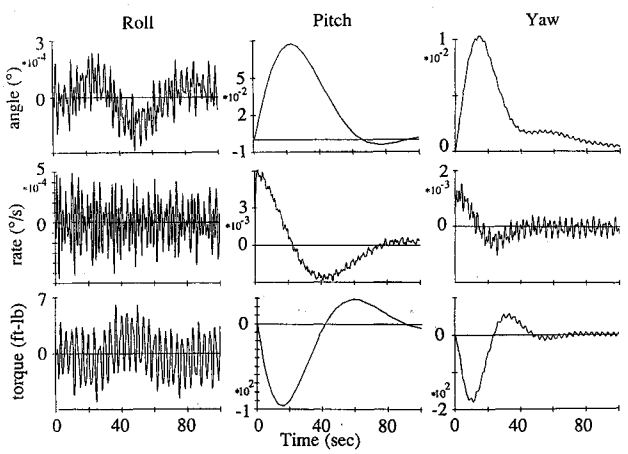

Fig. 10 Response of normal mode to impulsive crew disturbance.

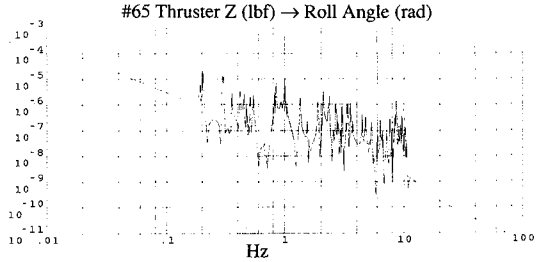

Fig. 11 Bode plot of no. 65 thruster (Z) to roll attitude.

configuration. Thrusters no. 65 and no. 102 have been moved toward the $-x$ direction by three bay lengths to allow adequate control authority.

Because the structural modes in Fig. 11 are closely spaced, it is not practical in the reboost mode to gain- or phase-stabilize any particular flexible mode. The approach used here is to settle on a low bandwidth and use a roll-off filter to attenuate all flexible modes. The RCS modes in this paper are limited to the completed phase 1 configuration. The controller should be able to adapt to earlier flights after flight 2 of Table 2 with gain scheduling, which will again probably be based on inertia. However, this aspect is not addressed in this study.

Reaction Control System Attitude Hold Mode

The deadband for attitude hold mode is set at 1 deg. This pointing accuracy allows a reasonably low rate of fuel consumption. The mode also effectively arrests rigid-body rates. For transition from RCS control into CMG control and other specialized position hold tasks, a tight RCS attitude hold mode has also been developed with deadbands of ± 0.1 deg on roll and yaw and ± 0.3 deg on pitch. For a controller with a Schmitt trigger and a minimum pulse width of 2 s, the residual rates are 0.003 deg/s on roll/yaw and 0.015 deg/s on pitch. If a PWPF with a 100 ms minimum pulse width is used, the residue rates should be 0.00015 deg/s or 20 times lower, allowing transition from RCS to CMG mode with no danger of CMG saturation. Stability analyses that include the effects of nonlinear switching logic show that the rigid-body mode has more than a 10 dB gain margin and 45 deg phase margin. All flexible modes have more than 10 dB gain margins.

Reboost Mode

Periodic orbit raising to compensate for drag loss is accomplished by thrust force toward the x direction. The attitude hold controller stops these thrusters for short intervals (off-modulation) and occasionally fires jets on orthogonal directions, to balance the net torques and direct the total thrust vector through the center of mass. A reorientation maneuver prior to reboost firings may be needed to align the net thrust in the desired ΔV direction. Each axis has a second-order roll-off filter with a corner frequency of 0.5 rad/s to attenuate high

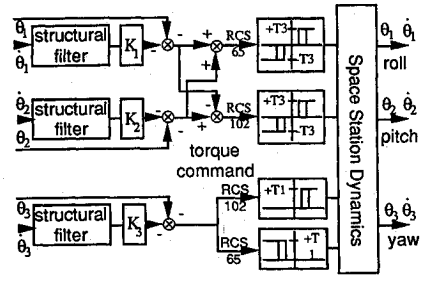

Fig. 12 RCS mode controller block diagram: Z thrusters for coupled roll/pitch control, X thrusters for yaw control.

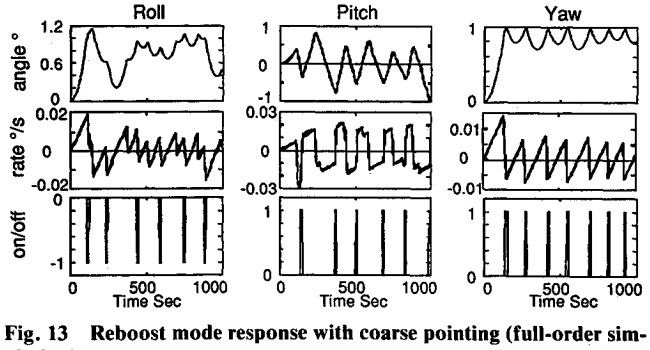

Fig. 13 Reboost mode response with coarse pointing (full-order simulation).

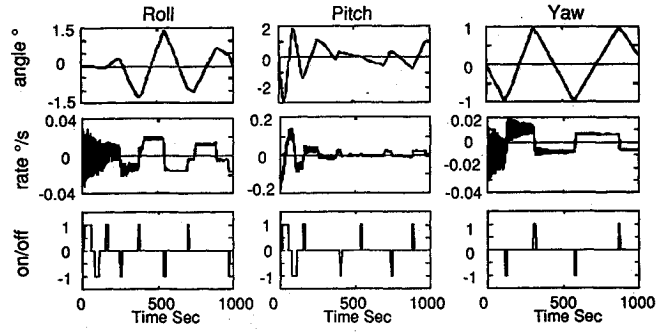

Fig. 14 Docking RCS response with ± 1 deg deadband (full-order simulation).

frequency modes. The closed-loop response of the reboost mode (Fig. 13, with a full-order model) shows cross-axis coupling and flexible mode excitation. Pointing accuracy of 1 deg is maintained.

Docking Mode

Normal mode is in operation before and during docking approach, while attitude hold mode operates in the background to unload the large docking impulse. A fully loaded Shuttle in hard docking has a 0.2 ft/s closing speed in the $-x$ direction. The docking port is on the $+x$ side of the module area. The net impulse of 1500 lb-s adds 13,000 ft-lb-s of momentum on both the pitch and yaw axes, which is close to the total CMG momentum capacity. The CMG mode responds to the sudden attitude rates with a peak torque of 800 ft-lb, which exceeds the CMG capability. Both facts indicate that CMGs cannot handle Shuttle docking without RCS. Figure 14 shows a simulation of docking transients with only RCS control. The roll and yaw attitudes are held within a ± 1 deg deadband, whereas the pitch attitude transient is less than 3 deg.

Summary

The use of traditional analysis and design tools in the preliminary design of the space station has been presented. Both collocated and noncollocated sensors and actuators are allowed. The topology of the controllers ensures robustness to plant variations. The large configuration changes during construction are handled by gain scheduling. The CMG mode achieves a moderate bandwidth. A common reaction jet controller serves attitude hold, reboost, CMG backup, and docking functions. In each case, the approach has successfully produced simple controllers that, when checked on the full-order model, exhibit satisfactory performance.

Acknowledgment

This paper was developed in part from work sponsored by NASA Marshall Space Flight Center (MSFC) under Contract NAS8-36422. Henning Krome of MSFC and John Sunkel of Johnson Space Center were technical monitors. Their support is greatly appreciated.

References

[1]Chu, P. Y., Wie, B., Gretz, B., and Plescia, C., "Control for an Evolving Space Station," Ford Aerospace, Palo Alto, CA, SSD-TR00103, March 1988.

[2]Schaeffer, H. G., *MSC/NASTRAN Primer,* Schaeffer Analysis, Mont Vernon, NH, 1979.

[3]Bernard, D., "Control System Design for Lightly Coupled Space Structures," Ph.D. Dissertation, Stanford Univ., Stanford, CA, Sept. 1984.

[4]Critical Evaluation Task Force (CETF) NASTRAN model, NASA Langley Research Center, Hampton, VA, June 1987.

[5]Anderson, B. D. O., and Liu, Y., "Controller Reduction: Concepts and Approaches," American Control Conference, Minneapolis, MN, June 1987, pp. 1-9.

[6]Bryson, A. E., Jr., "A Rapidly-Converging Algorithm for Optimal

Model Order Reduction of SISO System," American Astronautical Society 11th Annual Guidance and Control Conference, Keystone, CO, Jan. 30-Feb. 3, 1988.

[7]Bryson, A. E., Hermelin, S., and Sun, J., "LQG Controller Design for Robustness," American Control Conference, Seattle, WA, June 1986 (not in proceedings).

[8]Wie, B., and Byun, K. W., "A New Generalized Structural Filtering Concept for Active Vibration Control Synthesis," *Journal of Guidance, Control, and Dynamics,* Vol. 12, No. 3, 1989, pp. 147-154.

[9]Kennel, H. F., "Steering Law for Parallel Mounted Double-Gimbal Control Moment Gyros—Revision A," NASA TM-82390, Jan. 1981.

[10]Yeichner, J. A., Lee, J.F.L., and Barrows, D., "Overview of Space Station Attitude Control System with Active Momentum Management," American Astronautical Society 11th Annual Guidance and Control Conference, Keystone, CO, Jan. 30-Feb. 3, 1988.

[11]Wie, B., et al., "New Approach to Attitude/Momentum Control for the Space Station," *Journal of Guidance, Control, and Dynamics,* Vol. 12, No. 5, 1989.

[12]Wie, B., Hu., A., and Singh, R., "Multibody Interaction Effects on Space Station Attitude Control and Momentum Management," AIAA Paper 89-3514; also, *Journal of Guidance, Control, and Dynamics* (to be published).

[13]Wie, B., and Plescia, C. T., "Attitude Stabilization of a Flexible Spacecraft During Stationkeeping Maneuvers," *Journal of Guidance, Control, and Dynamics,* Vol. 7, No. 4, 1985, pp. 447-453.

[14]Kullas, M. C., "Handbook on Astronaut Crew Motion Disturbances for Control System Design," NASA RP-1025, 1979.